- 1 Empirical constraints on the mass dependence of isotope diffusion in
- 2 minerals by modeling sub-solidus exchange: Calcium isotopes in the
- 3 **two-pyroxene system**
- Zhihua Xiong ^a, Shichun Huang ^b, James A. Van Orman ^{a,*}
- ^a Department of Earth, Environmental and Planetary Sciences, Case Western Reserve University,
- 6 Cleveland, OH, USA
- 7 b Department of Earth and Planetary Sciences, University of Tennessee, Knoxville, TN, USA
- 8 *Corresponding author:
- 9 E-mail address: james.vanorman@case.edu
- 10 Abstract

23

Diffusion is a significant driver of isotope fractionation at high temperatures, but its precise role 11 is difficult to evaluate in many situations due to the sparsity of data on the isotopic mass 12 13 dependence of the diffusion coefficient. Such data are lacking particularly for diffusion in minerals. The ratio of diffusion coefficients of two isotopes of the same element in the same material can be 14 characterized as the inverse mass ratio raised to an empirical exponent β , but experiments to 15 determine β are challenging and few measurements have been reported. Here, a method is 16 developed to empirically determine β based on numerical modelling of the diffusion-controlled 17 elemental and isotopic redistribution between minerals during slow subsolidus cooling, and 18 comparison of the results to data from natural mineral pairs. The method is applied to the Ca 19 redistribution between orthopyroxene (opx) and clinopyroxene (cpx), where the elemental 20 partitioning equilibrium as a function of temperature has been well characterized experimentally 21 and Ca isotope fractionation data are available in natural samples that experienced slow cooling. 22

We show that the Ca isotope fractionation during cooling is insensitive to the initial temperature,

cooling rate or grain size over a broad range of conditions, provided that diffusion is sufficient to re-homogenize opx grains at near-peak temperatures during early cooling. Furthermore, we find that the Ca isotope fractionation established during cooling is much more strongly dependent on the value of β in opx than the value of β in cpx, as long as cpx dominates the Ca budget in the system. Transient heating events produce fractionation in the opposite sense to that developed during cooling, which can diminish or reverse the isotope fractionation for samples that experienced such events after cooling. Based on the largest Ca isotope fractionation that has been documented between opx and cpx in natural samples, it is inferred that for Ca, $\beta_{opx} = 0.04(1)$. Despite the relatively small inferred value of β_{opx} , diffusive fractionation of Ca isotopes between opx and cpx is significant over a broad range of cooling rates. Similar behavior during sub-solidus cooling is anticipated for other elements with temperature-dependent inter-mineral partition coefficients, and the method developed here has the potential to be used to place constraints on β for many elements, even in minerals where experimental measurements are not feasible.

- **Keywords:** Isotope fractionation; Mass dependence of isotope diffusion; Subsolidus redistribution;
- 38 Cooling rate; Closure temperature

1. Introduction

Isotopes of the same element generally diffuse at slightly different rates, due to their different masses. This dependence of the diffusivity on isotope mass can lead to significant isotope separation when there is net transport of an element via chemical diffusion: faster-diffusing light isotopes become concentrated in the region that an element diffuses toward, leaving behind a region that becomes relatively enriched in heavy isotopes. In contrast to equilibrium isotope fractionation, which diminishes rapidly as temperature increases (Urey 1947; Bigeleisen and Mayer, 1947), diffusive isotope separation persists at high temperatures (e.g. Richter et al., 2009,

2017; Van Orman and Krawczynski, 2015), and therefore may be particularly important for high temperature metamorphic and magmatic processes.

In order to evaluate the contribution of diffusion and make full use of diffusive isotope fractionation as a geochemical tool, it is critical to understand how strongly the diffusion coefficient depends on the mass of the isotope. An empirical function that is commonly used to describe the isotopic mass dependence of the diffusion coefficients in a particular phase is (Richter et al., 1999):

$$\frac{D_L}{D_H} = \left(\frac{m_H}{m_L}\right)^{\beta} \tag{1}$$

where D_L and D_H are the diffusion coefficients of the isotopes of mass m_L and m_H , and β is a dimensionless parameter. This equation is analogous to the one derived from the kinetic theory of an ideal gas, for which $\beta = \frac{1}{2}$ (Lasaga, 1998). In liquids and solids there is no simple theory for the value of β , although it is generally expected to have a value less than or equal to $\frac{1}{2}$. Instead, for each particular element in each mineral or liquid, the value of β must either be determined by experimental measurements (e.g., Richter et al., 2008; 2014; 2017; Watkins et al., 2009; 2011; Mueller et al., 2014; Fortin et al., 2017; Sio et al., 2018), calculated by theoretical simulations (Goel et al., 2012; Van Orman and Krawczynski, 2015), or constrained by empirical observations in natural samples (Sio et al., 2013; Oeser et al., 2015).

In minerals, it is often difficult to determine the β value experimentally because the diffusion profiles that can be generated in reasonable times are often too short to allow high-precision isotopic measurements along the diffusion profile. To date, experimental studies to determine β in minerals have been restricted to systems with relatively fast diffusion, including He in olivine and pyroxene (Trull and Kurz, 1993); C in iron (Müller et al., 2014); Li in pyroxenes (Richter et al.,

2014) and olivine (Richter et al., 2017); Fe and Ni in Fe-Ni alloys (Watson et al., 2016); and Fe in olivine (Sio et al., 2018). The value of β in a mineral depends on the statistics of the atomic jump sequence that leads to diffusion, and can be estimated based on information from independent experiments and/or first principles calculations (Van Orman and Krawczynski, 2015). However, there are few cases where sufficient information exists to make such estimates, and even fewer examples where these have been tested by experiments. Estimates of β from natural samples are also sparse, and have mainly been restricted to olivine phenocrysts in magmatic systems with well-defined thermal histories, where β_{Mg} and β_{Fe} in olivine have been estimated by fitting Fe and Mg isotopic profiles (Sio et al., 2013; Oeser et al., 2015).

Here, we develop a new method to determine β from natural samples, based on numerical modeling of isotopic diffusion profiles developed between two minerals during slow cooling. The method is applied to Ca isotopes in pyroxenes, where Ca is redistributed between high- and low-Ca pyroxene during subsolidus cooling, but has the potential to be applied to many other systems where the equilibrium distribution of an element between minerals is strongly temperature dependent.

2. Model description

We consider a system composed of orthopyroxene (opx) and clinopyroxene (cpx) grains that undergo subsolidus chemical and isotopic exchange during cooling (or heating). Because opx and cpx grains are commonly equant and there is little evidence for diffusional anisotropy (Cherniak and Dimanov, 2010), they are approximated as isotropic spheres. It is also assumed that the surfaces of opx and cpx maintain chemical and isotopic equilibrium at all times. Because opx and cpx grains are not in physical contact across their entire surfaces in an actual rock, this assumption implies the existence of a fast grain boundary network capable of accommodating the diffusive fluxes across the mineral surfaces to and from the grain interiors (e.g. Eiler et al., 1992). Although

that grain boundary" assumption is clearly a simplification, it seems reasonable to assume that grain boundaries can maintain efficient transport of Ca between opx and cpx surfaces given that (a) grain boundary diffusion in silicates (Farver et al., 1994; Dohmen and Milke, 2010) is many orders of magnitude faster than volume diffusion in pyroxenes (Cherniak and Dimanov, 2010; Zhang et al., 2010; Cherniak and Liang, 2022), and (b) Ca partitions strongly into grain boundaries (Hiraga et al., 2004), correspondingly increasing their transport capacity.

92

93

94

95

96

97

98

99

100

101

102

103

104

105

106

107

108

109

110

111

112

113

114

In our model, the system of opx and cpx grains begins in chemical and isotopic equilibrium and then undergoes subsolidus cooling, which disturbs the equilibrium. As the system cools, the concentrations at the mineral surfaces shift to maintain surface equilibrium, and this sets up concentration gradients within the mineral grains that lead to diffusional transfer of Ca and its isotopes from opx to cpx. Because diffusion slows as the temperature decreases, the system may move from a high-temperature regime in which bulk equilibrium is maintained and each grain is homogeneous in composition, through a disequilibrium regime in which the diffusional flux between opx and cpx is insufficient to achieve full equilibrium, to a final frozen regime where diffusional exchange has ceased. We consider the exchange of two different isotopes of Ca, ⁴⁰Ca and ⁴⁴Ca, which have slightly different diffusion rates due to their difference in mass. The mass dependence of the diffusion coefficients is characterized by the parameter β , as described above (Eq. 1). Temperature in the cooling simulations is assumed to decrease linearly from the initial temperature (T_i) to the final temperature (T_f) . We also performed simulations (not shown) in which temperature exponentially decreases with time, which yield similar results when the cooling rate is the same at the Ca exchange closure temperature.

As introduced above, we assume an equilibrium distribution of Ca isotopes between opx and cpx when cooling begins (t=0), with each grain internally homogeneous:

115
$$C_j^n(r_j, 0) = C_{j,0}^n$$
 $0 \le r_j \le R_j$ (2)

$$C_{opx,0}^n = K_{opx-cpx}^n C_{cpx,0}^n \tag{3}$$

where C is the concentration of Ca isotope n (n=40 represents 40 Ca and n=44 represents 44 Ca), the subscript j refers to the phase (opx or cpx), r is distance from the center of the grain, R is the outer radius of the spherical grain, and K is the partition coefficient between opx and cpx, which depends on temperature and isotope mass. For 40 Ca, we use the partition coefficient for Ca described by the thermodynamic model of Brey and Köhler (1990) (Table 1). We consider here isobaric cooling at a pressure of 1.5 GPa. At this pressure, the temperature dependence of 40 Ca partitioning between opx and cpx can be expressed as:

$$lnK_{onx-cnx}^{40}(T) = 2.76 \times 10^6 / T^2 - 1.16 \times 10^4 / T + 3.84$$
 (4)

For ⁴⁴Ca, we use the equilibrium isotope exchange equation determined by Wang et al. (2017). The authors found that the equilibrium Ca isotope fractionation between opx and cpx depends on the Ca concentration in opx (Wang et al., 2017), which is temperature-dependent. Including the effect of Ca concentration was found to have a negligible effect on the Ca isotope fractionation in our modeling (Fig. S1), so we assume the equilibrium Ca isotope fractionation between opx and cpx is only a function of temperature (Wang et al., 2017):

$$lnK_{opx-cpx}^{44}(T) = 6.46 \times 10^3 / T^2 + lnK_{opx-cpx}^{40}(T)$$
 (5)

We also assume that the grain boundary region is homogeneous, and that the cpx/grain boundary partition coefficient is equal to one, so that the initial Ca isotope concentration in the grain boundary (denoted by subscript *b*) is equal to that in the cpx:

135
$$C_{b,0}^n = C_{cpx,0}^n$$
 (6)

The assumption that the cpx/grain boundary partition coefficient is equal to one is arbitrary and has no influence on the results, because we set the grain boundary volume to be so small that its contribution to the Ca budget in the system is negligible.

The cpx rim (at outer radius *R*) is assumed to maintain chemical and isotopic equilibrium with the opx rim and with the grain boundary at all times:

$$C_{opx}^{n}(R,t) = K_{opx-cpx}^{n}(T)C_{cpx}^{n}(t)$$
(7)

$$C_{cnx}^n(R,t) = C_h^n(t) \tag{8}$$

- As temperature changes, the equilibrium concentrations at the interface also change, and this sets up the concentration gradients that drive diffusion in the grain interiors.
- The isotopic concentration within each grain of opx and cpx follows Fick's second law in spherical coordinates (Crank, 1975):

147
$$\frac{\partial c_j^n}{\partial t} = D_j^n(T) \left(\frac{\partial^2 c_j^n}{\partial r_j^2} + \frac{2}{r_j} \frac{\partial c_j^n}{\partial r_j} \right)$$
 (9)

where the parameter *D* is the diffusion coefficient, which is a function of the temperature and hence is a function of time during cooling. The temperature dependence of the diffusion coefficient for each isotope in each mineral is given by an Arrhenius equation:

151
$$D_j(T) = D_{0,j}e^{-\frac{E_j}{RT}}$$
 (10)

152

153

154

155

where D_0 is the pre-exponential factor, R is the ideal gas constant, and E is the activation energy. Although it has been found that Ca diffusivity in cpx is slightly anisotropic (e.g., Dimanov and Ingrin, 1995; Dimanov and Jaoul, 1998; Zhang et al., 2010), we assume here for simplicity that Ca diffusion in both opx and cpx is isotropic, and we adopt the Arrhenius parameters experimentally determined by Zhang et al. (2010) for cpx. The diffusion coefficient for Ca in opx is described using the Arrhenius relationship recently measured by Cherniak and Liang (2022) (Table 1).

The Ca diffusion parameters discussed above are applied to 40 Ca, the most abundant isotope. The diffusivity of 44 Ca is then determined by the exponent β :

$$D_j^{44} = D_j^{40} \left(\frac{40}{44}\right)^{\beta_j} \tag{11}$$

Because β for Ca diffusion has not been determined for either opx or cpx, we examine a full range of values in our modeling. Although β may depend on temperature (Van Orman and Krawczynki, 2015), this dependence is expected to be small and we assume here that β is constant in the temperature interval considered in this work. With respect to Eq. 10, this means that the isotopic mass dependence only appears in the pre-exponential factor, and that the activation energies are identical for both isotopes.

A mass balance constraint is implemented at each time step:

168
$$\frac{d}{dt} \left(\sum_{j} N_{j} \int_{0}^{R_{j}} 4\pi r_{j}^{2} C_{j}^{n} dr_{j} + V_{b} C_{b}^{n} \right) = 0$$
 (12)

where N_j represents the number of grains of each mineral j, the integral is over each grain's entire radius from the center (r=0) to the rim (r=R), and V_b is the volume of the grain boundary network, which is designated to be small enough that the grain boundaries make a negligible contribution to the Ca budget of the system. It was verified that changing V_b below this small value has no influence on the results. Equation (12) states that the bulk Ca isotope concentrations remain constant at all times in the closed system considered in our model. This mass balance equation is applied along with the interface equilibrium conditions (Eq. 4-8) in order to set the boundary condition at the surface of each cpx and opx grain at each time step. With this boundary condition,

and the diffusion equations (Eq. 9-11), the Ca isotope concentrations at the surface of each grain are calculated simultaneously with the radial distributions within each grain at each time step.

For simplicity, we assume that the modal proportions and grain radii ($R_{\rm opx}$, $R_{\rm cpx}$) of opx and cpx remain constant during cooling. In real cooling systems, the equilibrium proportions of opx and cpx do change during subsolidus cooling. However, this change is not large and, as discussed below, we find that the simulation results are insensitive to the modal proportions over a wide range as long as cpx dominates the Ca budget. Our primary focus is on systems with a substantial fraction of cpx, because such systems are the ones that have been investigated in terms of Ca isotope fractionation (Huang et al., 2010; Kang et al., 2016, 2020; Zhao et al., 2017; Chen et al., 2018; 2019; Dai et al., 2020). For most of the model results presented below, we assume opx:cpx proportions of 7:3, typical of lherzolites, but a wider range of phase proportions is also explored (Table 1). We assume that opx and cpx have the same grain size.

For a chosen cooling rate (dT/dt), initial temperature (T_i) and grain size (R), the isotopic concentration at position r within a grain at time t, represented by $C^n(r,t)$, is calculated by solving Eqs. 2-12 using a Crank-Nicholson finite difference formulation programmed with Matlab. The accuracy of the calculations depends on the number of radial grid points and time steps, with a denser sampling mesh requiring a longer computation time. For the simulations reported here, we use 500 radial grid points and 500 time steps, which yields nearly identical results to those obtained with finer sampling meshes.

The isotopic ratio profiles in opx and cpx grains at each time step are represented by:

197
$$\delta_j^{44/40} Ca(r,t) = \left[\left(\frac{C_j^{44}(r,t)/C_j^{40}(r,t)}{C_j^{44}/C_j^{40}} \right) - 1 \right] * 1000$$
 (13)

where C^{44}/C^{40} is the bulk isotope ratio of the whole system.

The bulk isotopic compositions in opx and cpx at time $t(M^n(t))$ are calculated by integrating the concentration over each grain:

201
$$M_j^n(t) = \int_0^R 4\pi r_j^2 C_j^n(r_j, t) dr_j$$
 (14)

and the magnitude of Ca fractionation between opx and cpx at a given time is represented as:

203
$$\Delta^{44/40} C a_{opx-cpx}(t) = 1000 * \ln \left(\frac{M_{opx}^{44}(t)/M_{opx}^{40}(t)}{M_{cpx}^{44}(t)/M_{cpx}^{40}(t)} \right)$$
 (15)

3. Results

The redistribution of Ca and its isotopes between opx and cpx depends on the grain size and the cooling rate, and may also depend on the initial temperature. Because the distance (x_D) an atom diffuses is proportional to the square root of time $(x_D \propto \sqrt{t})$, changing the grain radii in the model is equivalent to changing the cooling rate squared. For example, doubling the grain radii while keeping all other parameters constant yields exactly the same results as increasing the cooling rate by a factor of four. For the purpose of illustration, we keep the grain radii constant (1 mm) in the results shown below, and vary the cooling rate over a wide range. The results can be translated easily to different grain radii, by considering their proportionality with the square of the cooling rate.

3.1 Cooling driven element and isotope redistribution

An example of the model Ca concentration and isotope fractionation profiles generated in opx and cpx grains during cooling is shown in Fig. 1. At the highest temperatures, the diffusivity is fast enough that the system is capable of developing a new chemical equilibrium, as shown by the homogeneous elemental distribution profiles in the coexisting crystals during the early stage of cooling (Fig. 1a). However, as cooling progresses and diffusion becomes slower, opx and cpx fail

to fully re-equilibrate, and diffusional zoning profiles develop as Ca is transferred from opx to cpx. Eventually, the diffusivity becomes so slow that the concentrations in coexisting grains no longer change with further cooling. The time evolution is depicted in Fig. 1b, where the real model temperature (T_{real}) is plotted alongside the apparent equilibrium temperature (T_{app}) recorded by the ⁴⁰Ca distribution between opx and cpx. Initially the apparent temperature tracks the real temperature, and finally the apparent temperature becomes frozen-in as Ca is no longer redistributed between the opx and cpx grains. This final "frozen" apparent temperature can be defined as the closure temperature for the ⁴⁰Ca redistribution between opx and cpx, and the closure time is the time along the cooling path that this temperature corresponds to. For the example shown in Fig. 1, the closure temperature for ⁴⁰Ca exchange between opx and cpx is ~850 °C. As Ca is transferred from opx to cpx during cooling, Ca isotopes separate due to their massdependent diffusivity. An example of the resulting isotope fractionation is shown in Fig. 1(c, d), where it is assumed that $\beta = 0.05$ for both opx and cpx. Similarly to the Ca elemental exchange, the Ca isotope distribution between opx and cpx initially follows the equilibrium isotope exchange curve, deviates from it at lower temperature, and finally plateaus when diffusional exchange between the minerals ceases. Because Ca is transferred from opx to cpx during cooling, heavier Ca isotopes are preferentially retained in the opx due to their slower diffusivity. Hence, diffusive fractionation produces opx with a heavier Ca isotopic composition, and cpx with a lighter Ca isotopic composition. The measured isotope fractionation primarily reflects the deviation of $\delta^{44/40}$ Ca_{opx} from that of the bulk. Because cpx contains most of the Ca, $\delta^{44/40}$ Ca_{cpx} $\cong \delta^{44/40}$ Ca_{bulk}; opx, the minor phase in terms of the Ca distribution, controls the diffusive fractionation.

Accordingly, as discussed below, we find that the isotope fractionation of Ca is relatively

insensitive to the values of β for cpx, but strongly dependent on the value of β for opx.

220

221

222

223

224

225

226

227

228

229

230

231

232

233

234

235

236

237

238

239

240

241

242

3.2 Effects of cooling rate/diffusion rate/grain size and initial temperature

243

244

245

246

247

248

249

250

251

252

253

254

255

256

257

258

259

260

261

262

263

264

265

In a petrological system undergoing cooling, the closure temperature has a strong dependence on the cooling rate and grain size (Dodson, 1973; Eiler et al., 1992) and may also depend on the initial temperature (Ganguly and Tirone, 1999). Hence, one might anticipate that the diffusive isotope fractionation during cooling also depends significantly on these parameters. To examine the relationship between the diffusive isotope fractionation and the cooling rate, we performed a series of model runs with cooling rate varying over a wide range, between 1 °C/Myr and 1×10⁷ °C/Myr. As above, these models consider opx and cpx grains 1 mm in radius, with an initial temperature of 1200 °C and with β =0.05 assumed for both opx and cpx. The results are summarized in Fig. 2, which shows the Ca isotope fractionation between opx and cpx during cooling as a function of the apparent temperature (i.e. the temperature inferred from the bulk ⁴⁰Ca distribution between opx and cpx, if the distribution reflected chemical equilibrium). The minimum apparent temperature at the end of each curve represents the closure temperature. Perhaps surprisingly, we find that the final isotope fractionation is insensitive to the cooling rate (and to the closure temperature) between 1 °C/Myr and 10^2 °C/Myr, with a nearly constant value of $\Delta^{44/40}$ Ca_{opx-cpx} $\approx 1.52\%$ at the end of simulations at these cooling rates. At faster cooling rates, the degree of Ca isotope fractionation does depend significantly on the cooling rate: $\Delta^{44/40}$ Ca_{opx-cpx} results are calculated to be 1.4% and 0.31%, at 10^3 °C/Myr and 10^7 °C/Myr, respectively. It is important to note that the behavior of Ca isotopes during cooling differs from that of oxygen isotopes, where the final isotope distribution between minerals always depends strongly on the cooling rate (Eiler et al., 1992; Giletti, 1985). The fundamental difference is that the oxygen elemental concentrations in silicate minerals do not change appreciably with temperature, so there is no significant chemical diffusion of oxygen. Because the net elemental oxygen fluxes between minerals are negligible, diffusive fractionation of O isotopes during sub-solidus cooling is anticipated to be small. Although O isotope diffusion gradients must develop during cooling, and diffusive fractionation must occur if O diffusion is mass-dependent, these gradients are small and are not expected to produce large diffusive fractionation effects as in the case of Ca where there is significant chemical diffusion. Instead, the oxygen isotope distribution after cooling simply reflects the closure temperature, which depends on the cooling rate. In contrast, Ca undergoes substantial chemical exchange between minerals during cooling, which can result in strong diffusive isotope fractionation. Our results demonstrate that when isotope fractionation is primarily a result of chemical diffusion, there is not necessarily a strong dependence on cooling rate (or grain size), as there is for oxygen isotope fractionation, or for temperature-dependent elemental distributions. Furthermore, when there is significant diffusive fractionation of isotopes, the final isotopic composition may not reflect equilibrium at any temperature that the rock actually experienced on its cooling path.

The magnitude of diffusive isotope fractionation is expected to be proportional to the diffusional flux of Ca within the disequilibrium temperature interval. In Fig. 3a, the total mass transfer of Ca from the opx to the cpx, within the disequilibrium interval, is plotted as a function of the cooling rate. The disequilibrium temperature range considered in these calculations extends from the temperature (T_d) at which the Ca exchange temperature begins to deviate from the actual temperature (by greater than 0.1%), to the final temperature (T_f), at which the Ca exchange is frozen. The disequilibrium Ca flux first increases with cooling rate, because the disequilibrium interval shifts to higher temperatures where a larger mass transfer of Ca from opx to cpx is required to establish equilibrium. Beyond a cooling rate of ~10² °C/Myr the Ca flux decreases with cooling rate, as the freezing temperature of the Ca exchange rises and approaches the initial temperature.

Similar to the flux, the diffusive Ca isotope fractionation (blue circles in Fig. 3b) first increases and then decreases with cooling rate, with a peak at $\sim 10^2$ °C/Myr. This suggests that the Ca flux, in the disequilibrium regime, is the primary control on the extent of diffusive Ca isotope fractionation. The total diffusive isotope fractionation at the end of the simulation (pink circles in Fig. 3b) also includes the effect of the equilibrium isotope fractionation curve. With increasing cooling rate, the diffusive isotope fractionation curve departs from the equilibrium curve at progressively higher temperatures, i.e. from a progressively lower starting point. This has the effect of modulating the variation in isotope fractionation due to the changing Ca flux, keeping the isotope fractionation nearly constant at slow cooling rates. Because other isotope systems, and other mineral pairs, have broadly similar features – with equilibrium isotope fractionation diminishing with temperature, and with concave-downward solvus curves – we would expect broadly similar behavior in other systems, with a low sensitivity of the isotope fractionation to cooling rate at slow cooling rates. In detail, however, the behavior is not expected to be exactly the same in every system, and needs to be considered on a case by case basis. The time evolution of the isotope profiles in opx (Fig. 4) also provides insight on the effect of cooling rate. At cooling rates between 1 °C/Myr and 10² °C/Myr (shown in Fig. 4a-c), the primary change is the temperature interval over which diffusive isotope fractionation occurs. For example,

289

290

291

292

293

294

295

296

297

298

299

300

301

302

303

304

305

306

307

308

309

310

311

change is the temperature interval over which diffusive isotope fractionation occurs. For example, as shown in Fig. 1(d), at 10 °C/Myr, diffusive fractionation develops between ~1070 °C and ~690 °C, whereas at 1 °C/Myr and 10^2 °C/Myr, diffusive fractionation develops in the temperature range of ~950 °C - ~650 °C, and ~1190 °C - ~750 °C, respectively (Fig. S2). However, during these disequilibrium temperature intervals the Ca isotope profiles developed in the opx are very similar, with high $\delta^{44/40}$ Ca at the center of the opx grain becoming progressively lighter toward the rim (Fig. 4a-c). The isotope fractionation is sensitive to the cooling rate/grain size only when the

cooling rate is fast enough to limit diffusive fractionation at the center of the grain (Fig. 4d-h). At cooling rates greater than 10^3 °C/Myr, the temperature (T_d) at which Ca isotope fractionation departs from the equilibrium fractionation path is higher than the initial temperature (1200 °C), which leads to the failure of opx to develop a homogenous isotopic profile at the highest temperatures when cooling begins. As a result, the isotopic profiles develop a humped shape with the largest fractionations near the rim instead of centered at the core of the opx grain. With increasing cooling rate, less of the opx interior is affected by diffusive isotope fractionation, and the hump in the isotopic profile shifts further toward the rim, affecting less and less of the grain interior (Fig. 4e-h). The bulk isotopic fractionation between opx and cpx correspondingly decreases, as seen in Fig. 2. The model results presented above suggest that the initial temperature may play an important role in the diffusive isotope fractionation at high cooling rates. To better understand this dependence, we calculated the extent of Ca isotope fractionation as a function of cooling rate and initial temperature (Fig. 5). As above, the radii of opx and cpx grains are 1mm, and β =0.05 is used for both opx and cpx. Together, the results in Fig. 5a and 5b show that the isotope fractionation is insensitive to the initial temperature and to the cooling rate, as long as the closure temperature is substantially below the initial temperature (by ~ 150 °C or more for an initial temperature of 1000 °C, and by ~300 °C for an initial temperature of 1400 °C). We find, similarly to Ganguly and Tirone (1999), that the closure temperature depends on the initial temperature when the cooling rate is rapid, and/or the initial temperature is low. Further, we find that the regime where the closure temperature is independent of the initial temperature closely coincides with the regime where the

diffusive isotope fractionation between opx and cpx is independent of the initial temperature and

312

313

314

315

316

317

318

319

320

321

322

323

324

325

326

327

328

329

330

331

332

333

334

the cooling rate.

The results shown in Fig. 5 are critical for interpreting the isotope fractionation preserved in natural opx:cpx pairs that have undergone monotonic cooling. They demonstrate that if the closure temperature indicated by the elemental Ca distribution is sufficiently below the initial temperature, the diffusive isotope fractionation is independent of the cooling rate. In these cases, it is not essential to know the precise cooling rate the sample experienced in order to interpret the Ca isotope fractionation between opx and cpx.

It is important to emphasize that the insensitivity to cooling rate of Ca diffusive isotope fractionation between opx and cpx does not necessarily extend to other isotope systems or to other mineral pairs. Diffusive isotope fractionation during cooling-driven sub-solidus exchange depends on the diffusion parameters in the minerals and on the temperature dependence of element and isotope partitioning. The sensitivity to cooling rate must be examined by detailed modeling on a case by case basis.

3.3 Influence of β and modal proportions of opx and cpx

The examples shown above demonstrate that strong diffusive Ca isotope fractionation can be produced during cooling even when the isotope mass dependence of diffusion is quite small (β =0.05). In order to understand how the isotope fractionation depends on the mass dependence of the diffusion coefficient, we performed a set of simulations in which the β values for opx and cpx were varied over the full range that is physically relevant (i.e. from 0 to 0.5), while holding other parameters constant. We also examined systems with different proportions of opx:cpx, ranging from 9:1 to 1:9. These simulations were all performed in the "slow cooling" regime where the diffusive isotope fractionation is insensitive to the cooling rate, initial temperature or grain size. The results are shown in Fig. 6, for opx:cpx proportions of 7:3 and 3:7, and in Fig. S3 for proportions of 9:1 and 1:9.

The results in Fig. 6 show that the Ca isotope fractionation between opx and cpx is far more sensitive to $\beta_{\rm opx}$ than to $\beta_{\rm cpx}$, particularly when the fraction of cpx is large. These results can be understood in terms of the example shown in Fig. 1: because the bulk of the Ca in the system resides in the cpx, most of the isotope fractionation develops in the opx. The larger the cpx fraction, the less leverage it has on the isotopic fractionation. For opx:cpx proportions of 3:7, $\Delta^{44/40}$ Ca_{opx-cpx} is nearly independent of $\beta_{\rm cpx}$. These results indicate that $\beta_{\rm opx}$ can be best constrained in systems with large fractions of cpx (e.g. websterites and wehrlites). In systems with smaller cpx abundances, such as lherzolites or harzburgites, the Ca isotope fractionation that develops between opx and cpx during cooling would depend significantly on $\beta_{\rm cpx}$ as well, and hence constraints on $\beta_{\rm opx}$ would have larger uncertainty (absent independent knowledge of $\beta_{\rm cpx}$).

3.4 Diffusive isotope fractionation during heating

The temperature dependence of Ca partitioning between opx and cpx implies that diffusive isotope fractionation can be induced not only by cooling but also by heating. Because many mantle samples (xenoliths, for example) may have experienced transient heating, it is important to examine its effects. We performed simulations with temperature linearly increasing from 600 °C to a peak temperature of 1200 °C. For simplicity, and to illustrate the effects of heating in isolation, we assumed Ca to be homogeneously distributed in opx and cpx, and in chemical and isotopic equilibrium at the onset of heating.

Model results for a wide range of heating rates are shown in Fig. 7a. During the early period of heating, the diffusivity is not fast enough to allow Ca transfer, and hence no diffusive isotopic fractionation develops. At higher temperatures where Ca diffusion is significant, Ca is transferred from cpx to opx, because $K_{opx-cpx}^n$ has a positive temperature dependence. The faster diffusivity of the light isotope results in a progressively lighter isotopic composition in opx and a heavier

isotopic composition in cpx, and thus a decreasing $\Delta^{44/40}$ Ca_{opx-cpx}. As the temperature continues to increase, the diffusivity becomes faster, and may ultimately be fast enough to achieve an equilibrium isotope fractionation at high temperatures, depending on the peak temperature reached and the heating rate (Fig. 7a). Similar to the cooling process, the magnitude of Ca isotope fractionation along the heating path is controlled primarily by the isotope mass dependence of diffusion in opx (Fig. 7b).

Because heating produces isotope fractionation in the opposite direction to that produced during cooling, it could diminish or reverse the fractionation that developed during cooling. To estimate β_{opx} from natural samples, it is important to avoid samples that may have experienced late transient heating, and to consider samples with the maximum $\Delta^{44/40}\text{Ca}_{\text{opx-cpx}}$, which are likely to most faithfully preserve the isotope fractionation generated during slow cooling.

4. Discussion

4.1 Inference of β for Ca in orthopyroxene from natural samples

The results presented above show that diffusive exchange during cooling can fractionate Ca isotopes significantly between two pyroxenes, and that the fractionation is controlled primarily by diffusion in orthopyroxene. When cooling is sufficiently slow, the diffusive fractionation for Ca isotopes between opx and cpx is further shown to be insensitive to the cooling rate, grain size and initial temperature, and to depend primarily upon the mass dependence of isotope diffusion (β) for Ca in opx. Hence, it is possible to place constraints on β_{opx} based on the comparison of our model results to published Ca isotope data for slowly-cooled natural samples that contain two pyroxenes. The ideal samples for this purpose are those that (1) have cooled slowly enough that their frozen Ca exchange temperatures are well below their initial temperatures, so that the isotope

fractionation is nearly independent on the cooling rate; (2) have not experienced any re-heating, which could diminish or reverse the isotope fractionation that developed during cooling; and (3) contain a relatively large fraction of cpx, so that cpx dominates the Ca budget and the observed isotope fractionation is sensitive only to β_{opx} with a negligible influence of β_{cpx} . It is also essential that the minerals analyzed are pure, without inclusions that could affect their Ca isotopic compositions. Ideally, the zoning of Ca isotopic composition within the mineral grains would also be characterized, or Ca isotope data would be restricted to the cores of mineral grains where concentration gradients are negligible. Calcium isotope analyses have instead been performed primarily on opx and cpx mineral separates after crushing and sieving. Despite the lack of spatial context, published data still provide useful constraints on β_{opx} , as discussed below.

(Huang et al., 2010; Kang et al., 2016, 2020; Zhao et al., 2017; Chen et al., 2018; Dai et al., 2020) and samples from the mantle section of an ophiolite massif (Chen et al. 2019). The data are summarized in Fig. 8, where the Ca isotope fractionation between opx and cpx is plotted against the apparent equilibrium temperature recorded by the Ca elemental distribution. The samples span $\Delta^{44/40}$ Ca_{opx-cpx} values that are both above and below the equilibrium isotope fractionation curve. Most of the samples with relatively low apparent equilibrium temperatures (<900 °C) have values of $\Delta^{44/40}$ Ca_{opx-cpx} above the equilibrium fractionation curve, consistent with diffusive isotope fractionation during slow sub-solidus cooling. In contrast, many of the samples with high Ca exchange temperatures have $\Delta^{44/40}$ Ca_{opx-cpx} values that lie below the equilibrium isotope fractionation curve. These low values have been suggested to result from mineral-melt interactions during melt infiltration (e.g. Chen et al., 2018; Zhao et al., 2017). We note, however, that heating produces similar effects (see Fig. 7), and that the observed fractionation could potentially be

produced strictly by heating during melt infiltration, without accompanying mineral-melt interactions.

426

427

428

429

430

431

432

433

434

435

436

437

438

439

440

441

442

443

444

445

446

447

For the purpose of placing empirical constraints on β_{opx} , our focus is on samples with a simple slow cooling history, and with Ca exchange temperatures extending well below the initial temperatures of the samples. Websterites and lherzolites from the Balmuccia massif (BM) in the Ivrea zone of the Italian Alps (Chen et al. 2019) are inferred to have these properties. The BM lherzolites and websterites formed in the subcontinental lithospheric mantle (Mukasa and Shervais, 1999), with the websterites forming dykes that crystallized from pyroxene-saturated melts at high temperatures. The BM massif was then tectonically emplaced in the lower crust where it cooled slowly, over a period of at least 70 Myr (Peressini et al., 2007, and references therein), implying cooling rates of 10 °C/Myr or less. With crystallization temperatures for the websterites >1200 °C (Mazzucchelli et al., 2009), and opx-cpx Ca distributions reflecting equilibrium at ~840-900 °C (Fig. 8), it is clear that the BM samples cooled slowly enough to be in the cooling-rate-insensitive regime with respect to diffusive Ca isotope fractionation. The BM samples include two websterites with opx:cpx ~3:7, and two lherzolites with opx:cpx ~2:1. Our focus is on the websterites because their high proportion of cpx means that isotope fractionation is sensitive only to β_{opx} , whereas the lherzolites have some sensitivity to β_{cpx} (Fig. 6). In principle it is possible that Ca exchange with other phases could also contribute to the Ca isotope fractionation exhibited by the opx:cpx pair. However, the other minerals in the BM websterites (olivine and spinel) contain negligible Ca compared to opx and cpx. Hence, while diffusional Ca exchange with these minerals could have a strong influence on Ca isotope fractionation in olivine (or spinel), it would have negligible influence on the Ca isotopic compositions of opx and cpx.

Because the BM websterites (BM11-12 and BM11-14) studied by Chen et al. (2019) were collected from the same layer (Wang and Becker, 2015) and have a common thermal history, they should have similar extents of Ca isotope fractionation between opx and cpx. However, the intermineral Ca isotope fractionation of BM11-12 and BM11-14 are analyzed to be 0.72% and 1.29%, respectively (Fig. 8; Chen et al., 2019). Although Ca isotope zoning in opx grains is expected for slowly-cooled samples, with lower values near the rim (see Fig. 4), zoning is an unlikely explanation for this difference because each powder sample analyzed by Chen et al. (2019) integrated many grain fragments (they reported using 0.5-1 mm mineral grain separates, with 10-20 mg powdered for each analysis). Contamination of the opx separate with a small amount of cpx is one possible way to lower the measured isotope fractionation. The inclusion of ~1.5% cpx to the opx separate could explain the difference in isotopic composition between the two samples. To estimate β_{opx} we focus on the websterite sample with the largest opx-cpx fractionation (1.29%), because it is more likely to record the true isotope fractionation that developed during cooling. Assuming that the measured isotopic compositions for opx and cpx correspond to the bulk values integrated over entire grains, we can estimate the value of β_{opx} that produces $\Delta^{44/40}\text{Ca}_{\text{opx-cpx}} = 1.29\%$. This gives a value of $\beta_{\text{opx}} = 0.04(1)$, where the estimated uncertainty takes the full range of β_{cpx} (0-0.5) into account. This estimate of $\beta_{opx} = 0.04(1)$ could be considered a lower bound because it is possible that reheating could have reduced the Ca isotope fractionation developed during cooling, or that cpx inclusions in the opx analyzed by Chen et al. (2019) could have reduced the measured Ca isotope fractionation even in the sample with the largest measured isotope fractionation.

4.2 Comparison with other estimates for β in minerals

448

449

450

451

452

453

454

455

456

457

458

459

460

461

462

463

464

465

466

467

468

469

470

Although no prior experimental or theoretical study has estimated the isotopic mass dependence of Ca diffusion rates in orthopyroxene, β values have been determined in a few cases for other

elements in silicate minerals. On Fig. 9 our estimate of β for Ca in opx is compared to published data for He, Li, Mg and Fe in olivine and clinopyroxene. The data are plotted against the diffusion coefficient of the element at 1200 °C.

In crystals, the isotopic mass dependence of the diffusion coefficient depends on the sequence of atomic jumps and on the coupling of the diffusing atom to the vibrations of other atoms during a single jump, as given by the following expression (LeClaire, 1966; Van Orman and Krawczynski, 2015),

$$\left(\frac{D_L}{D_H} - 1\right) / \left[\left(\frac{m_H}{m_L}\right)^{\frac{1}{2}} - 1\right] = f\mathcal{K} \approx 2\beta$$
 (16)

where f is the correlation coefficient, and \mathcal{K} is the coupling constant, which typically has values close to one. Because simple interstitial diffusion is expected to have little to no correlation of successive atomic jumps, such that f has a value close to one, atoms that diffuse interstitially are expected to have strong isotopic mass dependence (large β), as well as relatively large diffusivity. On the other hand, diffusion by a vacancy mechanism, or by more complicated mechanisms involving interstitial and other sites, is often correlated (f < 1), which leads to a correspondingly smaller isotopic mass dependence. The data for Li and He shown in Fig. 9 (aside from He in clinopyroxene) generally appear to be consistent with diffusion by an interstitial mechanism. Mg and Fe in olivine have been inferred to diffuse by a vacancy mechanism (e.g. Dohmen et al., 2007) and consistent with this independent inference, have smaller values of β .

The small value we find for β_{opx}^{Ca} suggests that Ca diffusion in orthopyroxene involves significant correlation of successive atomic jumps. This is surprising because Ca is expected to diffuse more slowly than Mg, the predominant occupant of cation sites in orthopyroxene, and hence to have little to no correlation in the direction of successive jumps $(f \cong 1)$ if diffusion occurs by a vacancy

mechanism (Van Orman and Krawczynski, 2015). Correlation in the vacancy mechanism occurs when an atom makes back-and-forth exchanges with the same vacancy before the vacancy repositions itself around the atom. The higher frequency of Mg-vacancy exchanges, relative to Ca, would tend to randomize the position of a vacancy adjacent to the Ca atom before a Ca-vacancy exchange could occur, which would make diffusion by a vacancy mechanism nearly uncorrelated. The low value of β_{opx}^{Ca} suggests that Ca might not diffuse by a simple vacancy mechanism, but instead may have a more complicated sequence of atomic jumps, perhaps involving interstitial sites, that deviates significantly from an uncorrelated random walk. If Ca diffusion were uncorrelated, as expected for a vacancy mechanism with a slow-diffusing solute atom, the value of β_{opx}^{Ca} would be expected to be significantly larger – similar to Li – and Ca would be expected to develop much larger isotope fractionation between orthopyroxene and clinopyroxene during subsolidus cooling than has been observed in natural samples.

4.3 Potential applications of the approach to determine β in other systems

The approach demonstrated here has the potential for broad application to place empirical constraints on the isotopic mass dependence of diffusion for many elements in many different minerals. In general, the equilibrium partitioning of an element between two minerals is temperature-dependent, and isotope fractionation may develop due to chemical diffusion during cooling. The approach outlined here can be applied when the temperature-dependent chemical equilibrium has been well calibrated, the isotopic equilibrium exchange has been well-calibrated or can be inferred to be small, the elemental diffusion coefficients in the minerals have been characterized as functions of temperature, and data are available on the inter-mineral isotope fractionation in samples that have a simple, monotonic slow-cooling history. The method is particularly powerful when one of the two minerals is a minor host of the element under

consideration - as opx is for Ca when the opx:cpx ratio is not too large. In this case, the diffusive isotope fractionation between the two minerals is insensitive to the isotopic mass dependence of diffusion in the phase that is the primary host of the element. We have shown that the diffusive Ca isotope fractionation between opx and cpx is sensitive only to eta^{Ca}_{opx} - and insensitive to the cooling rate, grain size or initial temperature – when the cooling rate is slow enough to allow a stage of equilibrium exchange early in the cooling history, and the cpx fraction is large enough for it to dominate the Ca budget. The insensitivity we find to cooling rate/grain size has not been demonstrated for other element exchanges, and it may depend on the precise temperature dependence of the equilibrium elemental exchange and other factors. One example where the method outlined here appears to have significant potential is for the rare earth elements (REEs). The temperature dependence of the equilibrium REE exchange between opx and cpx has been well calibrated by Liang et al. (2013). Furthermore, the diffusion rates of REEs in opx (Cherniak and Liang, 2007) and cpx (Van Orman et al., 2001) have been measured experimentally. To our knowledge, equilibrium isotope fractionation has not been explicitly characterized through either experiments or theoretical calculations, but because the REEs have large atomic masses, it can be expected that the extent of equilibrium isotope fractionation of the REEs between opx and cpx is quite small (Bigeleisen and Mayer, 1947; Dauphas et al., 2018; Hu et al., 2021). Hence, the basis exists to estimate the isotopic mass dependence of the diffusivity for REEs in opx by modelling their diffusive isotope fractionation between opx and cpx during slow cooling, and comparing to their isotopic compositions in natural samples, which to our knowledge have not yet been determined. The method may also be applicable to sub-solidus exchange of REE

516

517

518

519

520

521

522

523

524

525

526

527

528

529

530

531

532

533

534

535

536

537

538

4.4 Do inter-mineral isotope distributions in high-temperature rocks reflect equilibrium?

for other mineral pairs, such as cpx and plagioclase/garnet.

Many studies have used natural samples to try to constrain equilibrium isotope fractionation between minerals at high temperatures (e.g. Chen et al., 2019; Williams et al., 2005). A critical underlying assumption in such studies is that the minerals (a) equilibrated isotopically at some temperature and then experienced negligible isotope exchange during cooling, or (b) experienced isotope exchange during cooling, but with a final distribution that reflects equilibrium at the closure temperature. We have shown that diffusion can produce strong disequilibrium isotope effects when there is significant elemental exchange between minerals due to temperaturedependent partitioning. These disequilibrium effects can be significant even when the mass dependence of isotope diffusion is fairly small, and are most apparent in minerals with low abundances of the element under consideration. Our modeling results show that for systems where the element partitioning between minerals depends significantly on temperature, isotope fractionation is likely to deviate significantly from equilibrium at the closure temperature, due to mass-dependent isotope diffusion. These disequilibrium effects would be avoided only if the elemental flux between minerals and/or the mass-dependence of isotope diffusion were negligible. Our results also show that disequilibrium diffusive fractionation can be significant even when cooling and/or heating rates are quite rapid.

5. Conclusions

539

540

541

542

543

544

545

546

547

548

549

550

551

552

553

554

555

556

557

558

559

560

561

A method was developed to estimate the isotope mass dependence of diffusion rate in crystals by modelling the diffusive redistribution between two minerals during slow sub-solidus cooling and comparing the results to the documented isotope fractionation in natural mineral pairs. The extent of diffusive Ca isotope fractionation between orthopyroxene and clinopyroxene is sensitive only to the isotopic mass dependence of the Ca diffusion coefficient in orthopyroxene, provided that clinopyroxene dominates the Ca budget and the Ca two-mineral exchange closure temperature is

well below the initial temperature at the onset of cooling. Heating can diminish or reverse the isotope fractionation developed during cooling. Comparison of the model results to published Ca isotope fractionation data from orthopyroxene: clinopyroxene pairs, β_{opx}^{Ca} is estimated to be 0.04(1). Even with this relatively small inferred value of β_{opx}^{Ca} , diffusive Ca isotope fractionation during slow subsolidus cooling is substantial, and in general the preservation of a high-temperature equilibrium isotope distribution is expected only if cooling is quite rapid. Similar effects are anticipated for other minor and trace elements that have temperature-dependent inter-mineral partition coefficients, and the method demonstrated in this study has the potential to be applied to estimate the mass dependence of isotope diffusion for a broad range of elements in a broad range of minerals.

References

Bigeleisen J. and Mayer M. G. (1947) Calculation of equilibrium constants for isotopic exchange reactions. *J. Chem. Phys.* **15**, 261-267.

Brey G. P. and Köhler T. (1990) Geothermobarometry in four-phase lherzolites II. New thermobarometers, and practical assessment of existing thermobarometers. *J. Petrol.* **31**, 1353-1378.

Chen C., Dai W., Wang Z., Liu Y., Li M., Becker H. and Foley S. F. (2019) Calcium isotope fractionation during magmatic processes in the upper mantle. *Geochim. Cosmochim. Acta* **249**, 121-137.

Chen C., Liu Y., Feng L., Foley S. F., Zhou L., Ducea M. N. and Hu Z. (2018) Calcium isotope evidence for subduction-enriched lithospheric mantle under the northern North China Craton. *Geochim. Cosmochim. Acta* 238, 55-67.

Cherniak D. J. (2001) Pb diffusion in Cr diopside, augite, and enstatite, and consideration of the dependence of cation diffusion in pyroxene on oxygen fugacity. *Chem. Geol.* **177**, 381-397.

Cherniak D. J. and Dimanov A. (2010) Diffusion in pyroxene, mica and amphibole. *Rev. Mineral. Geochem.* **72**, 641-690.

Cherniak D. J. and Liang, Y. (2007) Rare earth element diffusion in natural enstatite. *Geochim. Cosmochim. Acta* **71**, 1324-1340.

Cherniak D. J. and Liang, Y. (2022) Calcium diffusion in enstatite, with application to closure temperature of the Ca-in opx thermometer. *Geochim. Cosmochim. Acta.* https://doi.org/10.1016/j.gca.2022.06.018.

Coogan L. A., Kasemann, S. A. and Chakraborty, S. (2005) Rates of hydrothermal cooling of new oceanic upper crust derived from lithium-geospeedometry. *Earth Planet. Sci. Lett.* **240**, 415-424.

Crank J. (1975) The Mathematics of Diffusion. Clarendon Press, Oxford.

Dai W. Wang Z., Liu Y., Chen C., Zong K., Zhou L., Zhang G. L., Li M., Moynier F. and Hu Z. C. (2020) Calcium isotope compositions of mantle pyroxenites. *Geochim. Cosmochim. Acta* **270**, 144-159.

Dauphas, N., Hu, M. Y., Baker, E. M., Hu, J., Tissot, F. L., Alp, E. E., Roskosz, M., Zhao, J., Bi, W., Liu, J. and Lin, J. F. (2018) SciPhon: a data analysis software for nuclear resonant inelastic X-ray scattering with applications to Fe, Kr, Sn, Eu and Dy. *J. Synchrotron Rad.* 25, 1581-1599.

Dimanov A. and Ingrin J. (1995) Premelting and high-temperature diffusion of Ca in synthetic diopside: An increase of the cation mobility. *Phys. Chem. Miner.* **22**, 437-442.

Dimanov A. and Jaoul O. (1998) Calcium self-diffusion in diopside at high temperature: implications for transport properties. *Phys. Chem. Miner.* **26**, 116-127.

Dodson, M. H. (1973) Closure temperature in cooling geochronological and petrological systems. *Contrib. Mineral Petrol.* **40**, 259-274.

Dohmen R. and Milke R. (2010) Diffusion in polycrystalline materials: Grain boundaries, mathematical models, and experimental data. *Rev. Mineral Geochem.* **72**, 921-970.

Dohmen R. and Chakraborty S. (2007) Fe–Mg diffusion in olivine II: point defect chemistry, change of diffusion mechanisms and a model for calculation of diffusion coefficients in natural olivine. *Phys. Chem. Miner.* **34**, 409-430.

Dohmen R., Kasemann, S. A., Coogan L. and Chakraborty S. (2010) Diffusion of Li in olivine. Part I: experimental observations and a multi species diffusion model. *Geochim. Cosmochim. Acta* **74**, 274-292.

Eiler J. M., Baumgartner L.P. and Valley J.W. (1992) Intercrystalline stable isotope diffusion: a fast grain boundary model. *Contrib. Mineral. Petrol.* **112**, 543-557.

Farver J. R., Yund R. A. and Rubie D. C. (1994) Magnesium grain boundary diffusion in forsterite aggregates at 1000-1300 C and 0.1 MPa to 10 GPa. *J. Geophys. Res.* Solid Earth **99**, 19809-19819.

- Fortin, M. A., Watson, E. B. and Stern, R. (2017) The isotope mass effect on chlorine diffusion in dacite melt, with implications for fractionation during bubble growth. *Earth Planet. Sci. Lett.*, **480**, 15-24.
- Goel G., Zhang L., Lacks D. J. and Van Orman J. A. (2012) Isotope fractionation by diffusion in silicate melts: Insights from molecular dynamics simulations. *Geochim. Cosmochim. Acta* **93**, 205-213.
- Giletti B. J. (1985) The nature of oxygen transport within minerals in the presence of hydrothermal water and the role of diffusion. *Chem. Geol.* **53**, 197-206.
- Ganguly, J. and Tirone, M. (1999) Diffusion closure temperature and age of a mineral with arbitrary extent of diffusion: theoretical formulation and applications. *Earth Planet. Sci. Lett.* **170**, 131-140.
- Hiraga, T., Anderson, I. M. and Kohlstedt, D. L. (2004) Grain boundaries as reservoirs of incompatible elements in the Earth's mantle. *Nature*, **427**, 699-703.
- Hu, J. Y., Dauphas, N., Tissot, F. L. H., Yokochi, R., Ireland, T. J., Zhang, Z., Davis, A. M., Ciesla, F. J., Grossman, L., Charlier, B. L. A. and Roskosz, M. (2021) Heating events in the nascent solar system recorded by rare earth element isotopic fractionation in refractory inclusions. *Sci. Adv.* 72, p.eabc2962.
- Huang S., Farkaš J. and Jacobsen S. B. (2010) Calcium isotopic fractionation between clinopyroxene and orthopyroxene from mantle peridotites. *Earth Planet. Sci. Lett.* **292**, 337-344.
- Kang J. T., Zhu H. L. Liu Y. F. Liu F., Wu F., Hao Y. T., Zhi X. C., Zhang Z. F. and Huang F. (2016) Calcium isotopic composition of mantle xenoliths and minerals from Eastern China. *Geochim. Cosmochim. Acta* 174, 335-344.
- Kang J. T., Zhou C., Huang J. Y., Hao, Y. T., Liu F., Zhu H. L., Zhang Z. F. and Huang F. (2020) Diffusion-driven Ca-Fe isotope fractionations in the upper mantle: Implications for mantle cooling and melt infiltration. *Geochim. Cosmochim. Acta* **290**, 41-58.
- Lasaga A. C. (1998) Kinetic Theory in the Earth Sciences. Princeton University Press.
- Le Claire A. D. (1966) Some comments on the mass effect in diffusion. *Philos. Mag.* 14, 1271-1284.
- Mazzucchelli M., Rivalenti G., Brunelli D., Zanetti A. and Boari E. (2009) Formation of highly refractory dunite by focused percolation of pyroxenite-derived melt in the Balmuccia peridotite massif (Italy). *J. Petrol.* **50**, 1205-1233.
- Mueller T., Watson E. B., Trail D., Wiedenbeck M., Van Orman J. A. and Hauri E. H. (2014) Diffusive fractionation of carbon isotopes in γ -Fe: Experiment, models and implications for early solar system processes. *Geochim. Cosmochim. Acta* **127**, 57-66.
- Mukasa S. B., and Shervais J. W. (1999) Growth of subcontinental lithosphere: evidence from repeated dike injections in the Balmuccia lherzolite massif, Italian Alps. In *Developments in Geotectonics* (Vol. **24**, pp. 287-316). Elsevier.
- Oeser M., Dohmen R., Horn I., Schuth S., and Weyer S. (2015). Processes and time scales of magmatic evolution as revealed by Fe–Mg chemical and isotopic zoning in natural olivines. *Geochim. Cosmochim. Acta* **154**, 130-150.
- Peressini G., Quick J. E., Sinigoi S., Hofmann A. W., and Fanning M. (2007) Duration of a large mafic intrusion and heat transfer in the lower crust: a SHRIMP U–Pb zircon study in the Ivrea–Verbano Zone (Western Alps, Italy). *J. Petrol.* **48**, 1185-1218.
- Richter F. M, Chaussidon M., Watson E. B., Mendybaev, R. and Homolova, V. (2017) Lithium isotope fractionation by diffusion in minerals Part 2: Olivine. *Geochim. Cosmochim. Acta* **219**, 124-142.
- Richter F. M., Liang Y. and Davis A. M. (1999) Isotope fractionation by diffusion in molten oxides. *Geochim. Cosmochim. Acta* **63**, 2853-2861.
- Richter F. M., Watson, B. Chaussidon, M. Mendybaev, R. and Ruscitto, D. (2014) Lithium isotope fractionation by diffusion in minerals. Part 1: Pyroxenes. *Geochim. Cosmochim. Acta* **126**, 352-370.

- Richter F. M., Watson E. B., Mendybaev R. A., Teng F. Z. and Janney P. E. (2008) Magnesium isotope fractionation in silicate melts by chemical and thermal diffusion. *Geochim. Cosmochim. Acta* 72, 206-220.
- Sio C. K. I., Dauphas N., Teng F. Z., Chaussidon M., Helz R. T. and Roskosz M. (2013) Discerning crystal growth from diffusion profiles in zoned olivine by in situ Mg–Fe isotopic analyses. *Geochim. Cosmochim. Acta* **123**, 302-321.
- Sio, C. K., Roskosz, M., Dauphas, N., Bennett, N. R., Mock, T. and Shahar, A. (2018) The isotope effect for Mg-Fe interdiffusion in olivine and its dependence on crystal orientation, composition and temperature. *Geochim. Cosmochim. Acta*, **239**, 463-480.
- Schwandt C. S., Cygan R. T. and Westrich H. R. (1998) Magnesium self-diffusion in orthoenstatite. *Contrib. Mineral. Petrol.* **130**, 390-396.
- Trull T. W. and Kurz M. D. (1993) Experimental measurements of 3He and 4He mobility in olivine and clinopyroxene at magmatic temperatures. *Geochim. Cosmochim. Acta* **57**, 1313-1324.
- Urey H. C. (1947) The thermodynamic properties of isotopic substances. J. Chem. Soc. (Resumed), 562-581.
- Van Orman J. A., and Krawczynski M. J. (2015) Theoretical constraints on the isotope effect for diffusion in minerals. *Geochim. Cosmochim. Acta* **164**, 365-381.
- Wang W., Zhou C., Qin T., Kang J. T., Huang S., Wu Z. and Huang F. (2017) Effect of Ca content on equilibrium Ca isotope fractionation between orthopyroxene and clinopyroxene. *Geochim. Cosmochim. Acta* **219**, 44-56.
- Watkins J. M., DePaolo D. J., Huber C. and Ryerson F. J. (2009) Liquid composition-dependence of calcium isotope fractionation during diffusion in molten silicates. *Geochim. Cosmochim. Acta* **73**, 7341-7359.
- Watkins J. M., DePaolo D. J., Ryerson F. J. and Peterson B. T. (2011) Influence of liquid structure on diffusive isotope separation in molten silicates and aqueous solutions. *Geochim. Cosmochim. Acta* **75**, 3103-3118.
- Watson, H. C., Richter, F., Liu, A. and Huss, G. R. (2016) Iron and nickel isotope fractionation by diffusion, with applications to iron meteorites. *Earth Planet. Sci. Lett*, **451**, 159-167.
- Williams, H. M., Peslier, A. H., McCammon, C., Halliday, A. N., Levasseur, S., Teutsch, N. and Burg, J. P. (2005) Systematic iron isotope variations in mantle rocks and minerals: the effects of partial melting and oxygen fugacity. *Earth Planet. Sci. Lett*, *235*, 435-452.
- Zhao X., Zhang Z., Huang S., Liu Y., Li X. and Zhang, H. (2017) Coupled extremely light Ca and Fe isotopes in peridotites. *Geochim. Cosmochim. Acta* **208**, 368-380.
- Zhang X., Ganguly J. and Ito M. (2010) Ca–Mg diffusion in diopside: tracer and chemical inter-diffusion coefficients. *Contrib. Mineral. Petrol.* **159**, 175-186.

Table 1. Model Parameters

K ^a				$D_{0,opx}^{b}$ (m^2/s)	$D_{0,cpx}^{b}$ (m^2/s)	E _{opx} ^b (kJ/mol)	E_{cpx}^{b} (kJ/mol)	R (mm)	<i>T_i</i> (°C)	β	opx:cpx	Cooling rate (°C/Myr)	Heating rate (°C/Myr)
A ⁴⁰ (×10 ⁻⁶)	A ⁴⁴ (×10 ⁻⁶)	B (×10 ⁻⁴)	С	1.17×10 ⁻¹⁰	1.99×10 ⁻⁸	240	318.8	1	900 - 1400	0 - 0.5	1:9 - 9:1	10° - 10 ⁷	10 ⁰ - 10 ⁵
2.7635	2.7699	-1.16	3.84										

^a Parameters in opx/cpx partition coefficient. The temperature dependence of the partition coefficient (K) is expressed as: $lnK(T) = A/T^2 + B/T + C$. The parameters (A^{40} , B, C) describing the temperature dependence of $K^{40}_{opx-cpx}$ are based on the study of Brey and Köhler (1990). The parameters (A^{44} , B, C) describing $K^{44}_{opx-cpx}(T)$ are derived from the studies of Brey and Köhler (1990) and Wang et al. (2017).

^b Arrhenius parameters for diffusion coefficient $(D(T) = D_0 \exp(-\frac{E}{RT}))$. The temperature dependences of Ca diffusion coefficients in opx and cpx are described using the Arrhenius relationships experimentally determined by Cherniak and Liang (2022) and Zhang et al. (2010), respectively.

Figure captions

- **Figure 1.** Example model results for Ca exchange and isotope fractionation between opx and cpx, in a system with 1 mm radius grains cooling from 1200 °C (T_i) to 600 °C (T_i) at 10 °C/Myr. (a) Ca concentration profiles in opx and cpx (the inset shows Ca concentration profiles in cpx on a finer linear scale, so that the variation with temperature is evident). (b) Temperature and apparent temperature vs. time. The dashed line shows the actual temperature evolution considered in the model, and the solid curve shows the apparent temperatures recorded by the Ca elemental distribution between opx and cpx, where the Ca concentrations are integrated across the opx and cpx grains. (c) Ca isotope fractionation profiles across opx and cpx. The mass dependence of Ca isotope diffusivity is assumed to correspond to β = 0.05 for both opx and cpx. (d) Isotope fractionation between opx and cpx (integrated across the opx and cpx grains) as a function of temperature during cooling.
- **Figure 2.** The magnitude of diffusive Ca isotope fractionation between 1 mm opx and cpx grains, calculated as the system cools from 1200 °C to 600 °C at different cooling rates ($\beta_{opx} = \beta_{cpx} = 0.05$). T_{app} is the apparent temperature reflected by the elemental distribution of Ca between opx and cpx, along the cooling path. The results show that, when the system cools from 1200 °C, the magnitude of diffusive Ca isotope fractionation between opx and cpx is insensitive to the cooling rate, except when the cooling rate exceeds a threshold value. For 1 mm grains, the diffusive fractionation is insensitive to cooling rate below 1×10³ °C/Myr.
- **Figure 3.** (a) Ca flux out of opx from the departure temperature (T_d), where the Ca exchange temperature deviates from the actual temperature by 0.1%, to the final temperature (T_f), as a function of cooling rate. (b) Ca isotope fractionation between opx and cpx as a function of cooling rate. The blue circles show the diffusive isotope fractionation generated between T_d and T_f , and the magenta circles show the total isotope fractionation from the initial temperature (T_f) to the final temperature (T_f). Note that the difference between the blue and magenta circles at each cooling rate reflects the equilibrium Ca isotope fractionation at the departure temperature.
- **Figure 4**. The evolving Ca isotope profile in opx generated by diffusion, when system cools from 1200 °C at different cooling rates, (a-d) 10^{0} °C/Myr $\cdot 10^{3}$ °C/Myr; (e-h) 10^{4} °C/Myr- 10^{7} °C/Myr. The dashed line represents the initial Ca isotopic composition in opx when cooling begins (1200 °C). Solid curves denote the Ca isotope profiles in opx at different temperatures as cooling proceeds. The navy curve represents the $\delta^{44/40}$ Ca_{opx} profile in opx at the Ca diffusive exchange closure temperature.
- **Figure 5.** The dependences of (a) the Ca isotope fractionation between opx and cpx, at the end of cooling; and (b) the Ca closure temperature, on the initial temperature at the onset of cooling. Opx and cpx grain radii are 1 mm and β =0.05 is used for both minerals.
- **Figure 6**. The extent of Ca isotope fractionation, calculated as a function of the isotope mass dependences of the diffusion rates in opx and cpx (β in Eq. 11). The solid curves are for simulations with opx:cpx proportions of 7:3, and the dashed curves are for proportions of 3:7. The results are obtained using a cooling rate of 10 °C/Myr and grain radii of 1 mm.
- **Figure 7**. Ca isotope fractionation between opx and cpx during heating, as a function of (a) heating rate and (b) isotope mass dependence of the diffusion rate in opx and cpx. In (b) the shaded regions for each value of β_{opx} show the results obtained for β_{opx} in the range 0-0.25.
- **Figure 8**. Previously published data on the Ca isotope fractionation in opx-cpx pairs $\Delta^{44/40}$ Ca_{opx-cpx} plotted against the apparent equilibrium temperature recorded by Ca in opx. The $T_{\text{Ca-in-opx}}$ of Kang et al. (2016) and Kang et al. (2020) are the values given in those publications, and $T_{\text{Ca-in-opx}}$ of Huang et al. (2010), Zhao et al. (2017), Chen et al. (2018, 2019), and Dai et al. (2020) are calculated using the Ca-in-opx thermometer of Brey and Köhler, 1990. In the equilibrium

temperature calculations, the pressure is assumed to be 1.5 GPa. We note that a 0.5 GPa difference in pressure leads to a \sim 20 °C difference in temperature.

Figure 9. Our estimate of β for Ca in opx compared to published data for other elements in other silicate minerals. The β values are plotted against the diffusion coefficient of the chemical species at 1200 °C. These diffusion coefficients were obtained using the Arrhenius relationships determined in the following studies: He in olivine (ol) and diopside (cpx): Trull and Kurz (1993); Li in olivine: Dohmen et al. (2010); Li in diopside: Coogan et al. (2010); Mg and Fe in olivine: Dohmen and Chakraborty. (2007); Ca in orthopyroxene: Cherniak and Liang (2022). The difference between the diffusion rates of Fe and Mg in olivine in the studies of Sio et al. (2013) and Oeser et al. (2015) is accounted for by the different forsterite contents in their olivine samples.

Figures

Figure 1.

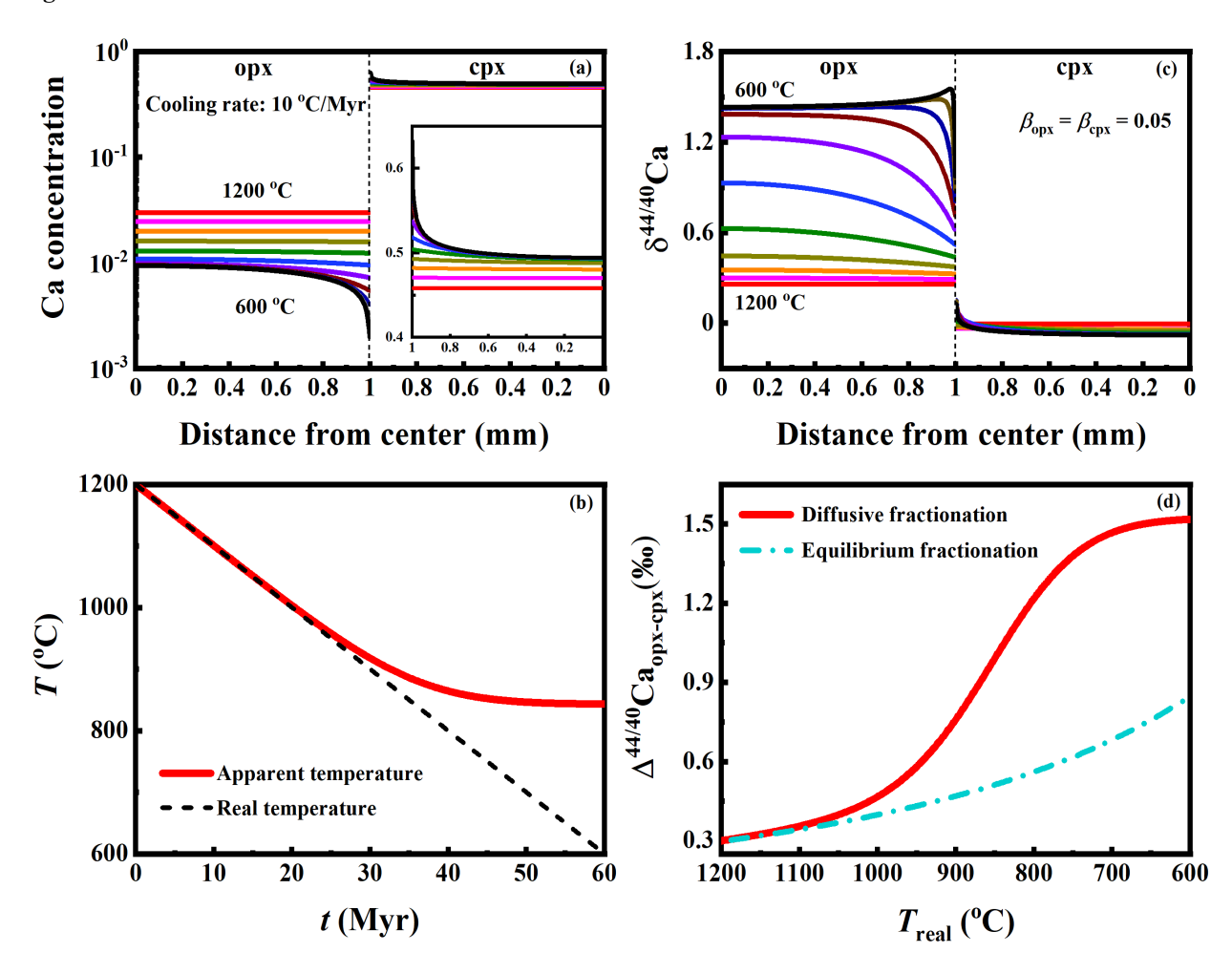


Figure 2.

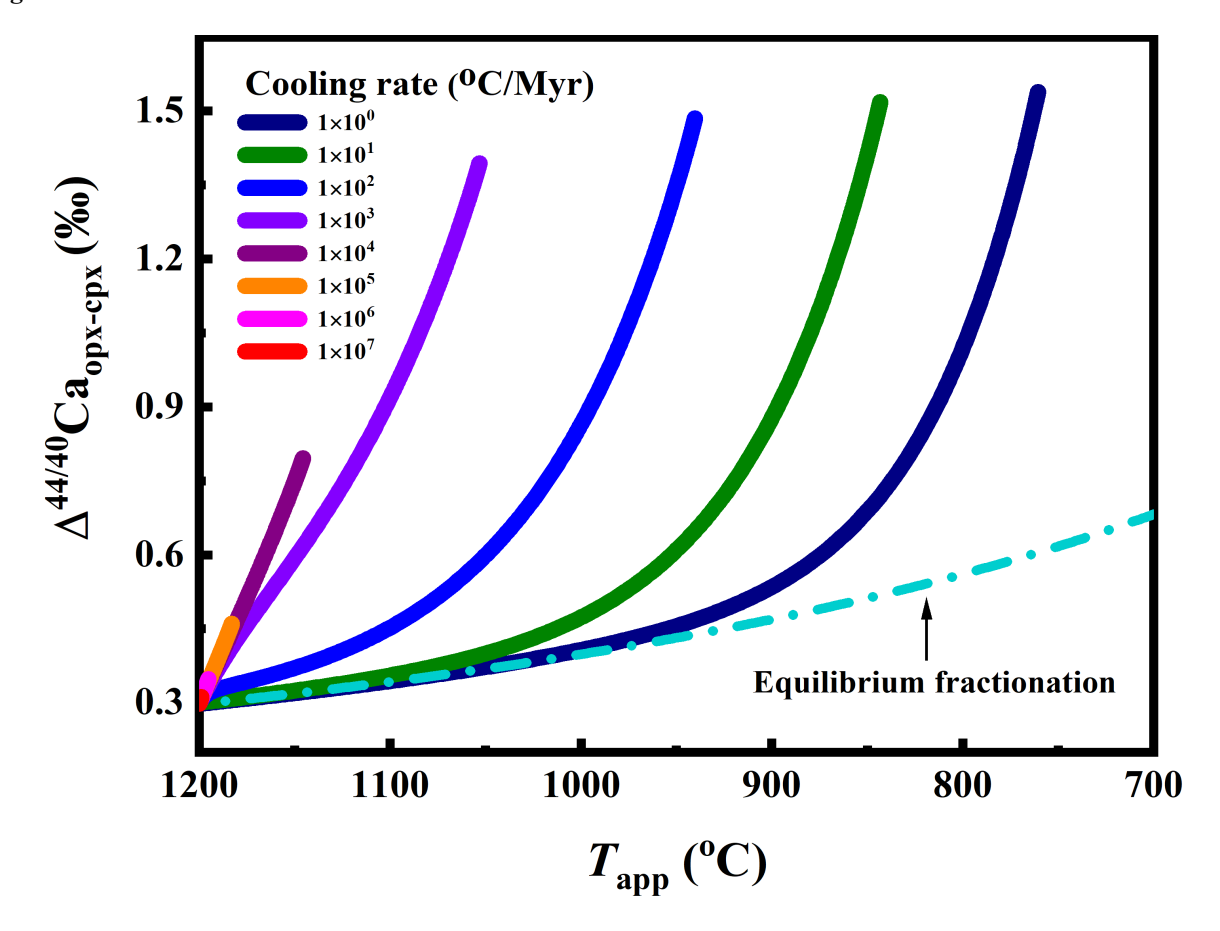


Figure 3.

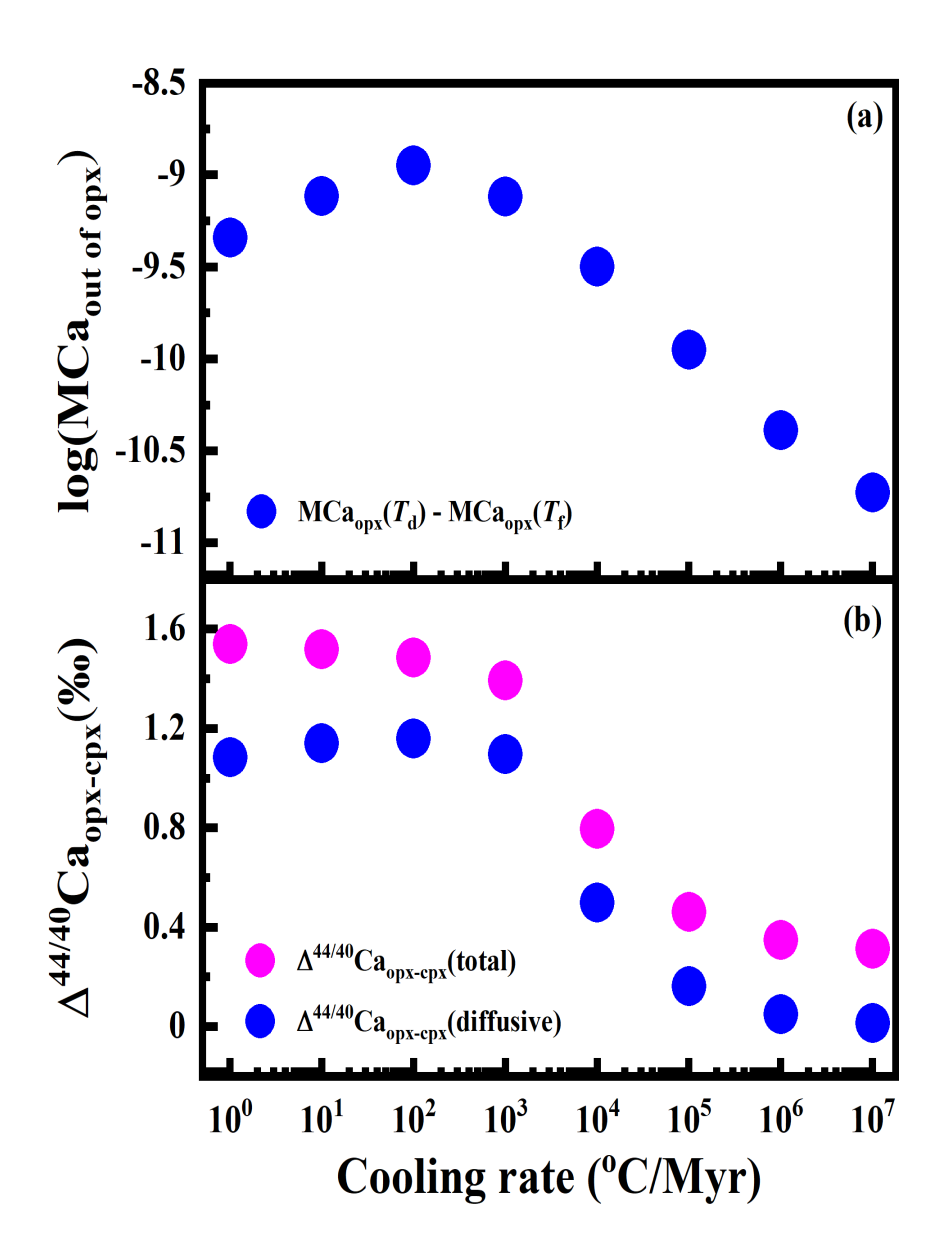
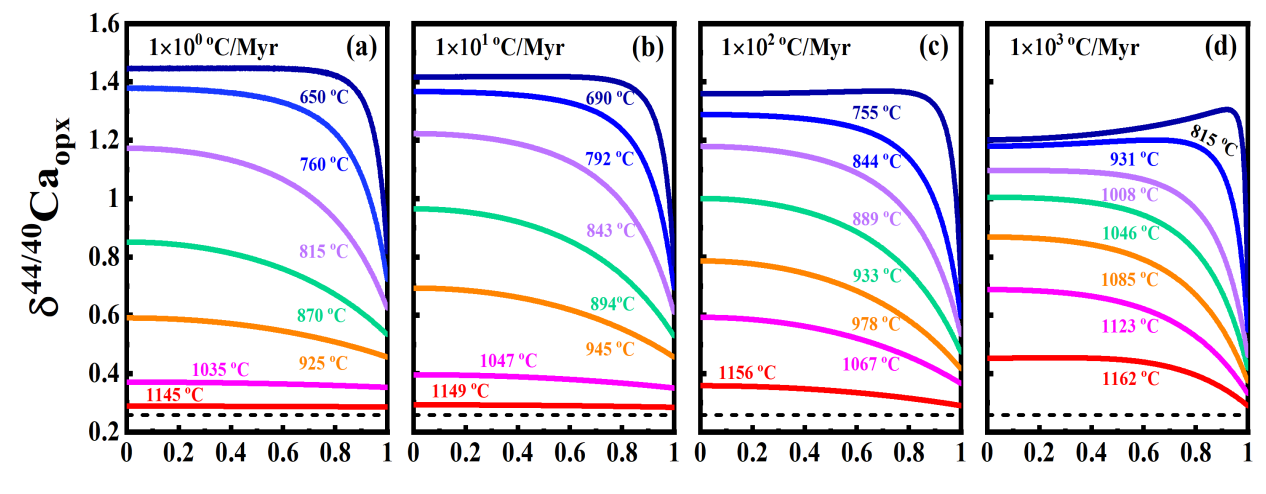
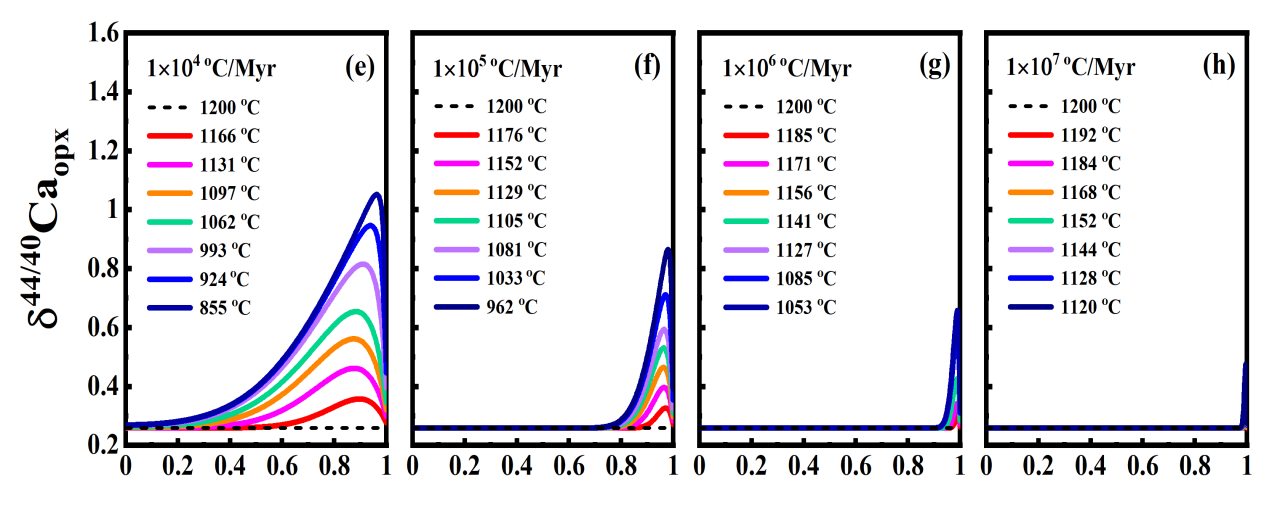


Figure 4.



Distance from center (mm)



Distance from center (mm)

Figure 5.

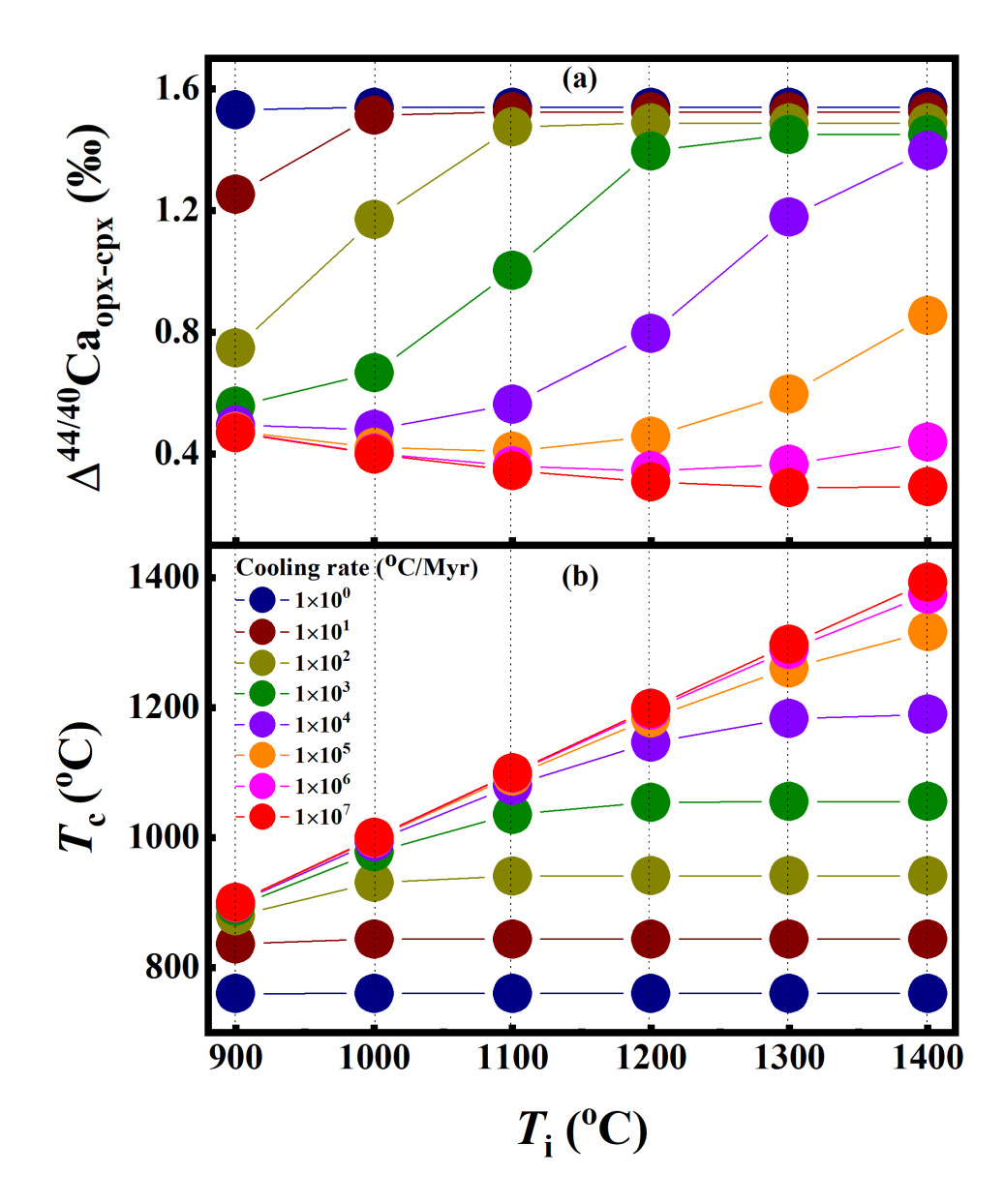


Figure 6.

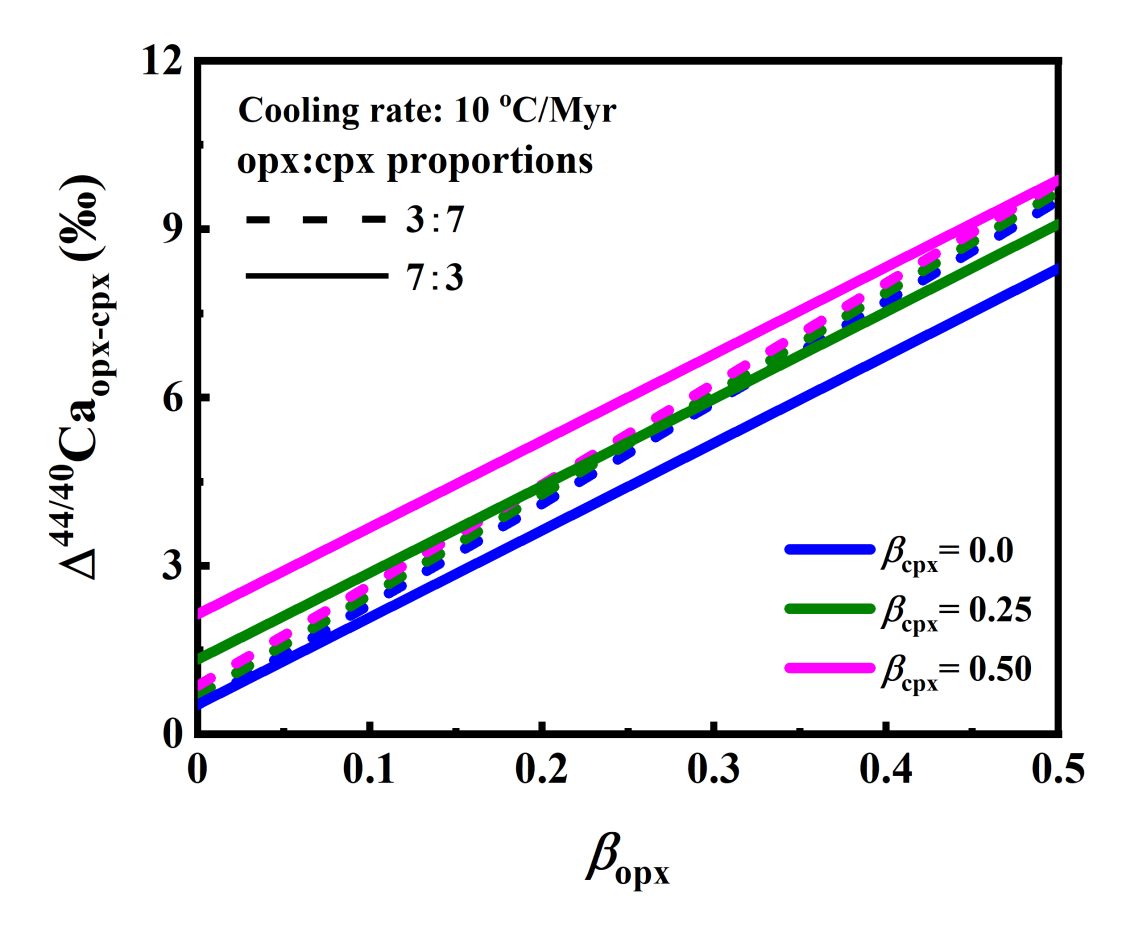


Figure 7.

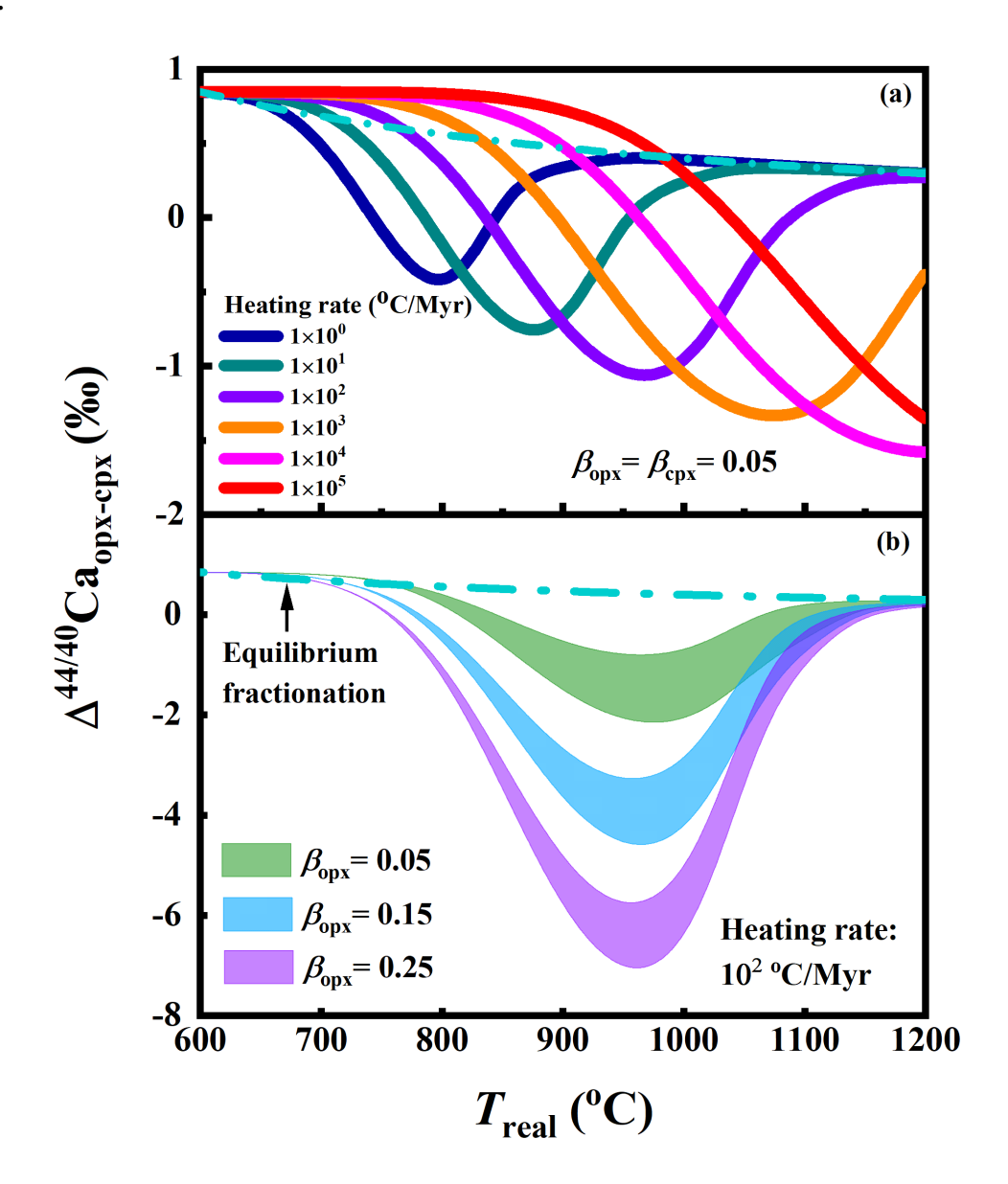


Figure 8.

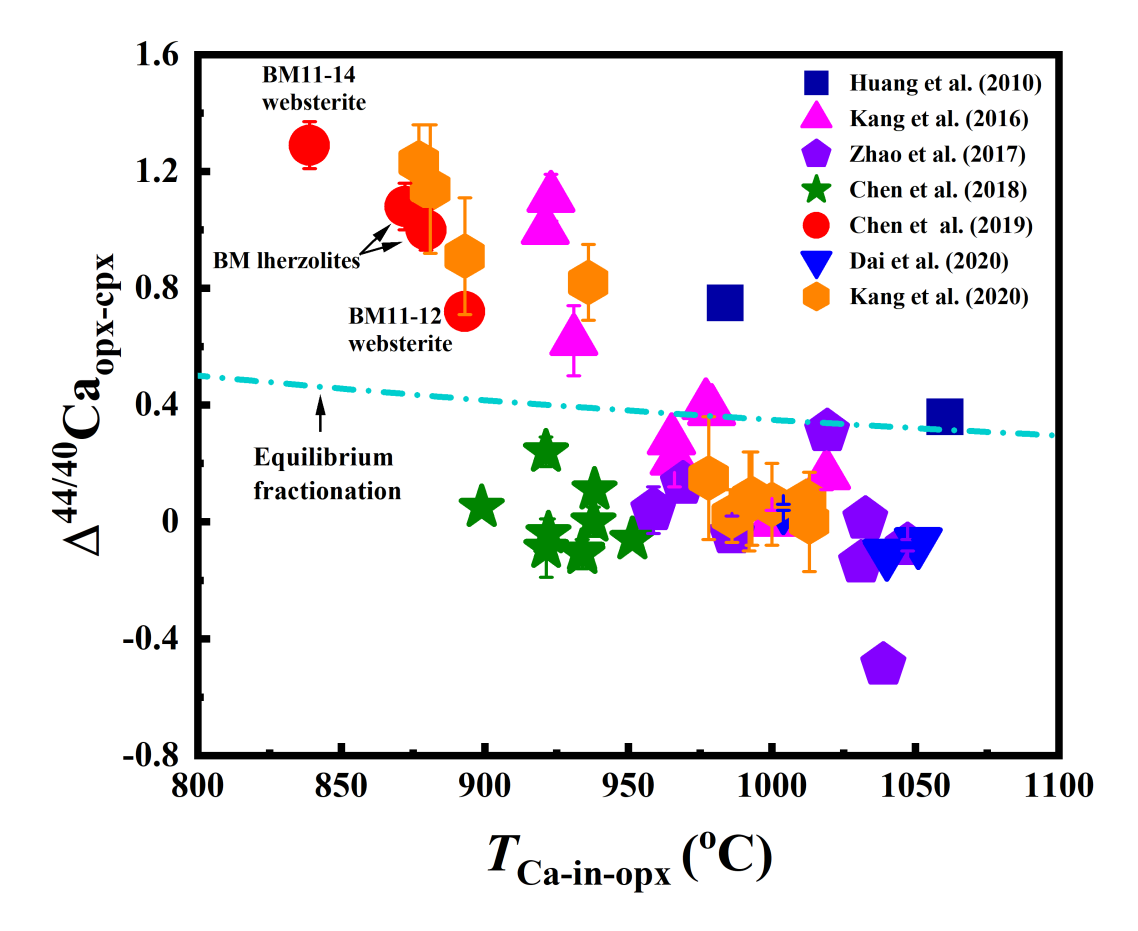


Figure 9.

